THE JOURNAL OF PHYSICAL CHEMISTRY A

pubs.acs.org/JPCA

Article

Not Completely Innocent: How Argon Binding Perturbs Cationic Copper Clusters

Zahra Jamshidi,* Olga V. Lushchikova, Joost M. Bakker,* and Lucas Visscher*

Cite This: *J. Phys. Chem. A* 2020, 124, 9004–9010

Read Online

ACCESS | Metrics & More | Article Recommendations | Supporting Information

ABSTRACT: Argon is often considered as an innocent probe that can be attached and detached to study the structure of a particular species without perturbing the species too much. We have investigated whether this assumption also holds for small copper cationic clusters and demonstrated that small but significant charge transfer from argon to metal changes the remaining binding positions, leading in general, to weaker binding of other argon atoms. The exception is binding to just one copper ion, where the binding of the first argon facilitates the binding of the second.

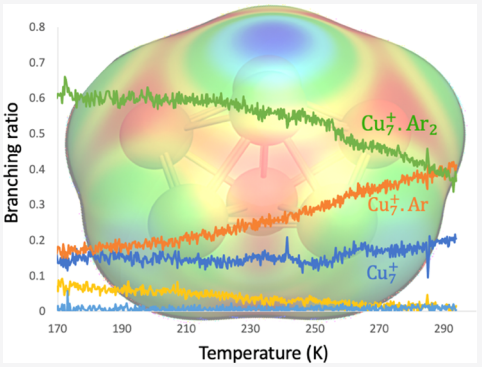

INTRODUCTION

Noble metal nanoparticles[1−9] have received significant attention in recent decades due to their unique electronic properties that make them interesting for a wide range of applications,[10−16] in particular, sensing[10,12] and catalysis.[13,16] If the number of atoms is small, these particles are highly symmetric and exhibit a significant energy gap between the highest occupied molecular orbital (HOMO) and the lowest unoccupied molecular orbital (LUMO). This is markedly different from the bulk and affects the chemical activity[17−21] of the nanoparticle by changing the affinity to store and release the electron density of adsorbed molecules.[21] While the structures and electronic properties of isolated small clusters can be readily studied by computational chemistry techniques, experimental validation of these data can be difficult as the cluster is often significantly perturbed by a cluster support or by the measurement itself. A powerful technique that allows the study of isolated but only weakly perturbed clusters is provided by infrared multiple photon dissociation (IRMPD) spectroscopy[22−28] with argon tagging atoms. Adsorption and desorption of noble gas atoms give only small perturbations of the cluster and can thus be used to characterize the structure of the bare metal clusters.[22−28] In an earlier study,[29] we have discussed such an application of IRMPD spectroscopy to determine the structure of cationic copper clusters, and we were able to unambiguously identify the lowest energy structures by comparison with IR spectra computed with density functional theory (DFT). This study did, however, reveal that for the smallest cationic clusters it is not valid to regard argon as just an inert probe as the tagging atom leads to a significant change in the computed IR spectra. In the current paper, we aim to study this interaction in more detail and furthermore rationalize the observed temperature-dependent product distribution of Ar adsorption onto Cu_n^+ clusters and the effect of finite temperatures on the IRMPD spectra.

The formation of bonds between noble gas atoms and noble metal clusters is fascinating as both species are considered inert in elementary chemistry textbooks. In the simplest picture, one expects bonding to be dominated by electrostatic and dispersion forces and to simply increase in strength when either the probing atom or the metal atoms are replaced by heavier, more polarizable, species. In a more refined picture, one considers also the spin state of the clusters and takes into account the possibility of forming coordination bonds.[30−38] Especially, for cationic noble metal clusters, charge transfer from the noble gas atom to the metal can be significant. An example is the unusually strong interaction of Ar with Au for mixed silver−gold trimer clusters. The perturbation induced by the noble gas atom gives rise to a significant change of their IR spectra relative to bare clusters.[39,40] The key ingredient of this effect is the relativistically enhanced electron affinity[41] of gold, which leads to the formation of a polar covalent bond[42] and significant charge transfer from argon to gold.[43] Since gold has the highest electron affinity (EA) among the coinage metals (EA_{Au} = 2.31 eV, EA_{Ag} = 1.30 eV, and EA_{Cu} = 1.23 eV),[44] one

Received: August 26, 2020
Revised: September 23, 2020
Published: October 15, 2020

https://dx.doi.org/10.1021/acs.jpca.0c07771
J. Phys. Chem. A 2020, 124, 9004–9010

would expect that this bonding is weaker for silver and still weaker for copper. Somewhat counterintuitively, we have found, however, that copper has a larger affinity to bind with rare gas atoms than silver. This makes this element an interesting target for further investigations.

In our previous study,[29] we discussed IRMPD spectra for Cu_n^+ (n = 3−10) clusters tagged with Ar atoms. In that study, we noted small, but important, effects of Ar atoms on the metal cluster IR spectra in the form of frequency shifting of the cluster modes and a strong enhancement of the cross-section for IR absorption. The additional peaks due to the motion of the Ar atoms themselves were not considered in that work and form the subject of the current study. We therefore also consider the experimentally more challenging, but theoretically easier, bonding of Ar to Cu^+ and the Cu_2^+ dimer to complete the picture. In this analysis, we aim to relate the thermodynamic stability of cluster−argon aggregates to the experimentally observed variation with the temperature of branching ratios between clusters tagged with different numbers of argon atoms. An additional analysis, using a Born−Oppenheimer molecular dynamics (BOMD), relates the details of the spectra that can be less well understood in a static picture to the mobility of argon atoms on the metal surface. Together, these analyses provide insight into how the binding of argon is influenced by the size and structure of the metal cluster and how the binding of one Ar atom may influence the binding of additional Ar atoms.

METHODS

Experimental Section. $Cu_n^+ Ar_m$ (n = 1−10; m = 1−4) clusters were generated in a clustering channel within a vacuum chamber using pulsed laser (532 nm) ablation in the presence of helium gas with 1% Ar admixed, let in through a pulsed valve (General valve Series 9) at a 7 bar stagnation pressure. The carrier gas pulse drives the clustering mixture through a 7 cm long, 4 mm diameter clustering channel that is temperature-controlled through a combination of liquid nitrogen (LN2) flow and resistive heating. The clustering channel ends with a converging−diverging nozzle, allowing mild expansion of the mixture into a vacuum, forming a molecular beam. This beam then passes a 2 mm diameter skimmer and a 1 mm diameter aperture, both slightly negatively biased to optimize cation transfer, to reach the extraction region of a reflectron time-of-flight mass spectrometer. After optional IR irradiation by a counterpropagating IR laser beam at frequencies of 70−300 cm^{-1}, all ions are pulse-extracted by applying high-voltage pulses on two parallel plate electrodes surrounding the molecular beam axis and mass-analyzed.

For temperature-dependent adsorption experiments, the cluster production was optimized by varying the synchronization of ablation laser timing and pulse energy with respect to the opening of the pulsed valve and mass extraction. The optimization was done such that, at all temperatures investigated, a substantial signal was observed. Once satisfactory conditions were found, the source was slowly cooled down to 150 K. To rule out hysteresis, the LN2 flow was stopped, and the source was slowly heated to room temperature. The temperature of the source was monitored using a thermocouple gauge.

The IRMPD spectrum was obtained by irradiating the cluster distribution using a free-electron laser, FELIX. Upon resonant absorption of IR photons, the weakest bond in the complex, the Cu_n^+ Ar bond, breaks, resulting in a decrease of the $Cu_n^+ Ar_m$ ion signal and a simultaneous increase of the $Cu_n^+ Ar_{m-1}$ ion signal. By recording the intensity changes of these mass peaks as a function of IR wavelength, IRMPD spectra were constructed. For details of the experiment, see Lushchikova[29] and references therein.

Computational Studies. Structures were taken from our previous work.[29] We calculated static vibrational frequencies with ADF[45,46] using the Perdew−Burke−Ernzerhof (PBE) generalized gradient (GGA) exchange−correlation density functional[47,48] with the inclusion of the Grimme dispersion correction scheme (D3)[49,50] using Becke−Johnson damping[49−51] and a triple-ζ double polarized (TZ2P) Slater-type basis set.[52] Relativistic effects were accounted for by the zeroth-order regular approximation (ZORA).[53,54] ADF was also used for energy decomposition analysis (EDA)[55,56] of the optimized structures. This method[55,56] is used to decompose the energy of binding a single Ar atom to the rest of the cluster into three attractive and one repulsive term. For our purposes, we combine the attractive electrostatic (ΔV_{elstat}) and orbital interaction (ΔE_{oi}) terms as they together describe charge transfer and polarization. These terms are balanced by the repulsive Pauli (ΔE_{Pauli}) interaction. The fourth term is the parametrized attractive dispersion interaction that is calculated and tabulated separately. These binding energies are supplemented with the internal energy, calculated via the statistical thermodynamics analysis implemented in ADF, to obtain dissociation enthalpies at finite temperature.

Relativistic coupled-cluster calculations were carried out with the DIRAC program[57,58] using the molecular mean-field exact 2-component[59] transformed Dirac−Coulomb Hamiltonian and the (uncontracted) valence double zeta basis set of Dyall.[60] Thresholds for determining the occupied and virtual orbitals in the correlation calculation were kept at the default values of −10 and +20 Hartree, respectively, leading to the correlation of 19 electrons for each Cu and 14 electrons for each Ar.

To explore the potential energy surface away from the local minima, an ab initio Born−Oppenheimer molecular dynamics (BOMD) simulation[61] was carried out for the $Cu_7^+ Ar_3$ complex. We used canonical (NVT) sampling, a dispersion-corrected PBE functional,[49,50] and Gaussian basis sets (double-ζ DZVP) with Goedecker−Teter−Hutter (GTH)[62] pseudopotentials with a 420 Rydberg plane-wave cutoff value. The simulation was performed in a cubic box with sides of 24 Å. The time step in the simulation was 0.5 fs., the simulation length was 40 ps, and the temperature was 180 K. The IR spectrum (band positions, intensity, and shape) was obtained through a Fourier transform of the dipole time-correlation function. The BOMD simulation and trajectory evaluation to obtain IR spectra were performed with the CP2K v2.3[63] and TRAVIS[64] packages, respectively.

RESULTS AND DISCUSSION

Temperature Dependence. One of the parameters that experimentally can be varied to study the Ar complexation of Cu_n^+ clusters is temperature. While the adsorption reaction is not affected, the desorption efficiency varies with temperature. At low temperatures, the experimental mass spectra reveal the presence of clusters with up to four adsorbed argon atoms, whereas at higher temperatures, only clusters with one or two argon atoms are observed. To disentangle the adsorption process from the overall cluster production efficiencies, the

https://dx.doi.org/10.1021/acs.jpca.0c07771
J. Phys. Chem. A 2020, 124, 9004−9010

abundance of $Cu_n^+Ar_m$ complexes are presented in the form of branching ratios, calculated as the ratio of the intensity of a particular complex $Cu_n^+ Ar_m$ detected to the sum of intensities for all m values, representing the total number of clusters Cu_n^+ of a certain size n produced. Figure 1 shows the branching ratios of $Cu_n^+Ar_m$ (n = 1−7, m = 1−5) complexes as recorded with a 1% argon−helium mixture as a function of temperature. For the smallest clusters, the branching ratios vary strongly with temperature, while for Cu_5^+, the $Cu_5^+ Ar_3$ signal dominates the Cu_5^+ branch over the whole temperature range (150 to 295 K) considered. A similar observation is made for Cu_6^+ and Cu_7^+, where the argon uptake appears to stagnate at $Cu_6^+ Ar_2$ and $Cu_7^+ Ar_2$ with no significant signal of clusters with more argon atoms attached.

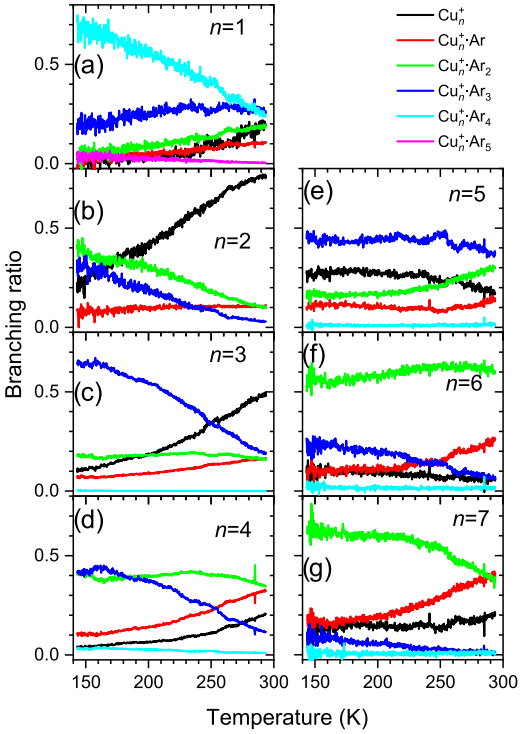

Figure 1. Branching ratios of $Cu_n^+Ar_m$ (n = 1−7, m = 1−5) complexes formed as a function of temperature for a 1% argon−helium mixture.

Thermodynamic Stability. The observed branching ratios can be related to the thermodynamic stability as a function of the number of Ar atoms attached to the clusters. We therefore computed the formation energy for the $Cu_n^+ Ar_m$ (n = 1−7; m = 1−n) complexes. The enthalpy $\Delta H_{n,m}$ needed to eliminate one Ar atom from a cluster containing n Cu atoms and m Ar atoms at 180 K is plotted in Figure 2 and also summarized in Table S1 (Supporting Information). Overall, one observes the expected gradual decrease of the magnitude of the dissociation energies as the number of Cu atoms increases and the average charge on the Cu atoms diminishes. Cu_4^+ Ar is an exception to this rule, as it more easily sheds its last argon than Cu_5^+ Ar. The plots furthermore show a grouping of the number of binding energies that is due to the equivalence of binding sites on these symmetric Cu clusters. For instance, in the D_{3h} symmetric Cu_3^+ cluster, all binding sites are initially equal and the small difference between $\Delta H_{3,1}$ $\Delta H_{3,2}$ and $\Delta H_{3,3}$ is caused by charge transfer to the Cu_3^+ core when Ar atoms are added. The contribution of the vibrations on dissociation enthalpies is small, at most 0.05 eV, so we can also discuss binding energies rather than enthalpies in the following when comparing DFT and confirmed by relativistic coupled cluster (CCSD(T)) values. The trend predicted with density function theory (DFT) using a dispersion-corrected exchange−correlation functional (PBE-D3) is confirmed by relativistic coupled cluster (CCSD(T)) calculations, which gave $|\Delta E_b^{Cu_3^+ Ar_3}|$(0.34 eV) < $|\Delta E_b^{Cu_3^+ Ar_2}|$(0.36 eV) < $|\Delta E_b^{Cu_3^+ Ar}|$(0.39 eV) (see Table S2).

The two largest clusters here (n = 6 and 7) predominantly bind two Ar atoms, which can be understood from the substantial decrease in binding enthalpy $\Delta H_{n,m}$ going from m =

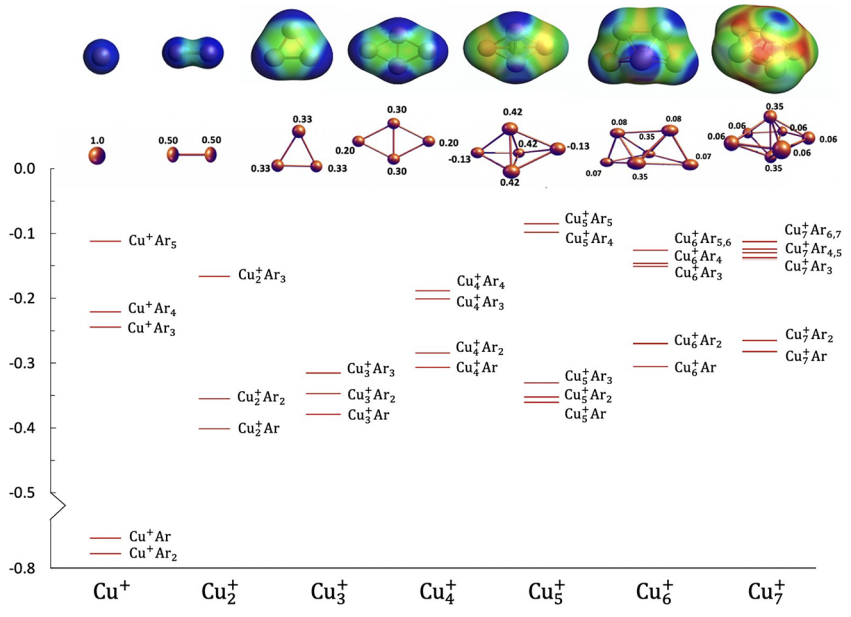

Figure 2. Comparison of the difference of enthalpy (in eV) for evaporating one Ar from each complex, $\Delta H_{n,m} = H_{n,m} - H_{n,m-1}$ (n = 1−7). Natural population analysis and electrostatic potential map of bare Cu_n^+ (n = 1−7) clusters.

https://dx.doi.org/10.1021/acs.jpca.0c07771
J. Phys. Chem. A 2020, 124, 9004−9010

2 to m = 3. For n = 5, the dominance of Cu_5^+ Ar_3 over the entire range of temperatures can similarly be related to the large difference in enthalpy in binding a third (−0.33 eV) or a fourth (−0.10 eV) Ar atom. The situation is different for n = 4, where the Cu_4^+ Ar_3 and Cu_4^+ Ar_2 complexes have nearly equal branching ratios over the 150 to 200 K temperature range. In this case, there is only a gradual decrease in binding enthalpy as the number of Ar atoms increases. The Cu_3^+ cluster, is able to strongly bind 3 Ar atoms, which explains the dominance of this species over the entire temperature range (see Figure 1). The 3-fold degeneracy of the binding sites in the equatorial plane of the Cu_5^+ cluster and the 2-fold symmetry of the axial sites in Cu_7^+ are similarly reflected in the corresponding binding energies. The calculated binding enthalpies again correlate well with the trends in the experimental branching ratios (Figure 1).

For Cu^+, theory predicts binding of up to 4 Ar atoms with affinities greater than 0.2 eV, which is in a reasonable agreement with an earlier experiment in which this cluster was observed to be the dominant species.[65] This extreme case also clearly illustrates the interplay between the Ar atoms: the first two atoms are predicted to bind with an affinity of about 0.6 eV at the CCSD(T) level of theory (Table S2). While DFT overshoots this value, both methods agree that the energy required for binding the second Ar is larger than that required for binding the first. This counterintuitive effect can be explained by the reduced Pauli repulsion that the second Ar atom encounters upon approaching Cu^+ Ar instead of a bare Cu^+ ion. For binding the first Ar atom, the unfavorable Pauli repulsion of 1.46 eV is overcome by energetically favorable polarization and charge-transfer interactions that amount to −2.25 eV. When binding the second atom, these polarization and charge-transfer interactions are smaller in magnitude (−2.06 eV), but this decrease is more than compensated by a still larger reduction in Pauli repulsion to 1.25 eV. This reduction can be understood by comparing the electron density of Cu^+ and Cu^+ Ar. The former is of course spherically symmetric with an equal probability of binding an Ar on either side, whereas Cu^+ Ar has a preformed binding site at the opposite side of the first Ar. The bonding affinity drops for the third and the fourth Ar and is only 0.1 eV for the fifth Ar. This is consistent with our experimental data pointing to Cu^+ Ar_4 as the dominant species in the temperature range below 270 K, with the weakly bound Cu^+ Ar_5 species being detected as well. For Cu_2^+, the interplay between binding multiple Ar atoms is less important because this species has two well-defined binding sites at opposite ends of the molecule, where Ar can donate electron density into the half-filled σ_g orbital of Cu_2^+. Binding the first Ar reduces the overall charge and thus diminishes the polarization and charge-transfer interactions, while not strongly affecting the Pauli repulsion (Table S3). This cluster can probably only support the binding of up to three Ar, and attaching the fourth yields a shallow minimum at the density functional level of theory (cf. SI).

For larger clusters, for which a detailed orbital analysis is more difficult, we focus only on charge transfer and polarization and identify preferred binding sites via a natural population analysis (NPA) of the charge distribution in bare clusters. This analysis (see Figure 2) reveals that the amount of charge localized on each Cu atom differs significantly and correlates well with three strong binding sites in Cu_5^+ and only two in Cu_7^+. Furthermore, we note that the highest local charges cannot be simply correlated with cluster size: $q_{Cu_5^+}(0.42) > q_{Cu_6^+}(0.35) \approx q_{Cu_7^+}(0.35) > q_{Cu_3^+}(0.33) > q_{Cu_4^+}(0.30)$. The exceptionally high local charge in the Cu_5^+ cluster is for the three Cu atoms in the equatorial plane that carry a positive charge of 0.42, whereas the two atoms along the vertex have even a slightly negative charge (about −0.13) in this analysis. For Cu_7^+, the population analysis shows a larger positive charge on the two apices (0.35) versus the equatorial plane (0.06). The slight weakening of bonding, which in general occurs for equivalent sites when one or more argon atoms are attached, can be understood by the charge that is transferred to the metal cluster due to the bonding. This can be quantified by carrying out an NPA for the Ar-tagged clusters (see Figures S1 and S2) and reveals that about 0.08 e is transferred, primarily to the Cu atom involved in the bond, also reducing the net positive charge on other binding sites. This generally correlates well with the decrease of desorption energy that is calculated. The charge transfer manifests itself furthermore in the alteration of the Cu−Cu bonds in the clusters. In our previous work, it was shown that neglecting the Ar and comparing the IR photodissociation spectra of Cu_n^+ Ar_m to the calculated spectra of bare Cu_n^+ clusters provided a substantially poorer match than with calculations in which Ar is considered. Bands associated with Cu_n^+ cluster vibrations were often blue-shifted in frequency, while IR cross-sections were amplified or became visible by symmetry breaking. The blue shift of Cu−Cu vibrations (in comparison to the isolated cluster) correlates with the decrease of Cu−Cu bond lengths (about 0.01 Å) induced by electron donation from the Ar atoms. This effect is most pronounced for smaller clusters; for the larger clusters, e.g., Cu_{10}^+ Ar, the IR spectra of isolated and complexed clusters in the range of metal vibrations (150−250 cm^{-1}) are nearly identical.

Focusing on the dominant electrostatic (charge-transfer and polarization) interactions between the rare gas and cationic noble metal clusters, the thermodynamic stability of a complex can be understood by considering the sites that have a sizeable localized charge. These are the only ones that are able to hold onto an Ar atom at elevated temperatures, and counting these sites provides a prediction for the dominant species for a certain cluster size. More shallow binding sites play a role at lower temperatures, and in this weak binding regime, Ar atoms can also show significant mobility. As this mobility can invalidate the time-independent DFT approach, in which only oscillations around well-defined minima are considered, it is of interest to consider the dynamics of the cluster explicitly. To this end, we turned to ab initio molecular dynamics and calculated the IR spectrum via the time-correlation function of the molecular dipole moment.

This approach, in which temperature effects are explicitly included, samples other parts of the potential energy surface than just the local minima associated with the specific binding sites of the Ar. In our previous work, the harmonic IR spectra for small Cu_n^+ (n = 3, 4, 5) clusters (tagged with Ar atoms) were compared with experiment, which provided a good match with the experimental data. This points to relatively rigid Cu_n^+—Ar bonds for these n values, which is consistent with the high local charge on each Cu in these clusters. In contrast to this good agreement, the harmonic IR spectrum for Cu_7^+ Ar_3 showed significant deviations from the experimental spectrum in the frequency region around 100 cm^{-1}, which relates to the Ar cluster bonds. We therefore focused on this cluster for our BOMD study. In Figure 3, the static harmonic and dynamic

https://dx.doi.org/10.1021/acs.jpca.0c07771
J. Phys. Chem. A 2020, 124, 9004−9010

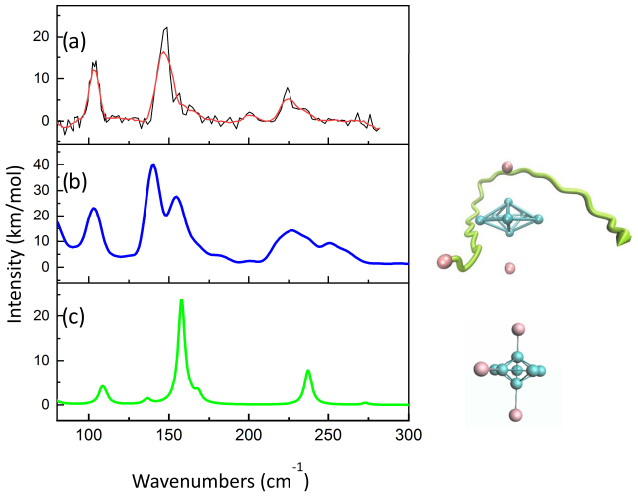

Figure 3. IR Spectra for the Cu_7^+ Ar_3 complex: (a) experimental IRMPD spectrum, (b) dynamic BOMD simulation at 180 K, and (c) static calculation (convoluted with a Lorentzian function of full width at half-maximum (FWHM) = 5 cm^{-1}).

BOMD IR spectra for Cu_7^+ Ar_3 were compared with experimental IR spectra.[29] From this Figure, it is clear that the BOMD IR calculations give better agreement with respect to the high-intensity peak at 100 cm^{-1}. Looking more closely at the trajectory that is used to generate the spectrum also reveals the cause of this difference relative to static DFT. For the two strong binding (q = 0.35) sites, the Ar atoms do indeed oscillate around a minimum energy structure, but the third Ar atom roams over the entire equatorial plane, visiting, in turn, the five shallow (q = 0.06) sites.

CONCLUSIONS

For small copper clusters, even the small perturbation of an absorbed Ar atom has a marked impact on the ability to bind subsequent species. The relative stability of specific Cu_n^+ Ar_m(n = 1−7) clusters as a function of temperature can be observed experimentally and can be related to the strength of the binding at different sites. Combining theory and experiment allows for a detailed understanding of the morphology of charge localization in Cu_n^+. The presence of additional shallow binding sites could be demonstrated by comparing low-temperature experiments to dynamic IR simulations.

ASSOCIATED CONTENT

Supporting Information

The Supporting Information is available free of charge at https://pubs.acs.org/doi/10.1021/acs.jpca.0c07771.

Calculated enthalpy of detaching an Ar atom from complex $\Delta H_{n,m}$ (m = 1−n); comparison of the binding energies, $\Delta E_b = E_{Cu_n^+}$ Ar-($E_{Cu_n^+} + E_{Ar}$), at different levels of theory; energy decomposition analysis for $Cu_{1,2}^+$ Ar_m interactions at the PBE-D3/TZ2P level of theory; optimized PBE-D3/TZ2P coordinates of Cu_n^+−Ar_m (n = 1−7) complexes; natural population analysis of bare clusters; natural population analysis of Cu_n^+−Ar (n = 3−7) complexes (PDF)

AUTHOR INFORMATION

Corresponding Authors

Zahra Jamshidi − *Chemistry Department, Sharif University of Technology, Tehran 11155-9516, Iran; Theoretical Chemistry, Vrije Universiteit Amsterdam, Amsterdam 1081 HV, the Netherlands;* orcid.org/0000-0003-0976-1132; Email: njamshidi@sharif.edu

Joost M. Bakker − *Institute for Molecules and Materials, FELIX Laboratory, Radboud University, 6525 XZ Nijmegen, the Netherlands;* orcid.org/0000-0002-1394-7661; Email: j.bakker@ru.nl

Lucas Visscher − *Theoretical Chemistry, Vrije Universiteit Amsterdam, Amsterdam 1081 HV, the Netherlands;* orcid.org/0000-0002-7748-6243; Email: l.visscher@vu.nl

Author

Olga V. Lushchikova − *Radboud University, Institute for Molecules and Materials, FELIX Laboratory, 6525 XZ Nijmegen, the Netherlands;* orcid.org/0000-0002-5699-6818

Complete contact information is available at: https://pubs.acs.org/10.1021/acs.jpca.0c07771

Notes

The authors declare no competing financial interest.

ACKNOWLEDGMENTS

This work is part of the Nederlandse Organisatie voor Wetenschappelijk Onderzoek (NWO) Materials for Sustainability program, funded under grant #739.017.008. We gratefully acknowledge NWO for the support of the FELIX Laboratory, and NWO-EW for computational time on the Cartesius computer cluster (grant 16327). Z.J. acknowledges the Holland Research School for Molecular Chemistry for a fellowship.

REFERENCES

(1) Kamei, Y.; Shichibu, Y.; Konishi, K. Generation of small gold clusters with unique geometries through cluster-to-cluster transformations: octanuclear clusters with edge-sharing gold tetrahedron motifs. *Angew. Chem., Int. Ed.* **2011**, *50*, 7442−7445.

(2) Biltek, S. R.; Mandal, S.; Sen, A.; Reber, A. C.; Pedicini, A. F.; Khanna, S. N. Synthesis and structural characterization of an atom-precise bimetallic nanocluster, Ag4Ni2 (DMSA) 4. *J. Am. Chem. Soc.* **2013**, *135*, 26−29.

(3) Chen, J.; Zhang, Q.-F.; Bonaccorso, T. A.; Williard, P. G.; Wang, L.-S. Controlling gold nanoclusters by diphosphine ligands. *J. Am. Chem. Soc.* **2014**, *136*, 92−95.

(4) McKenzie, L. C.; Zaikova, T. O.; Hutchison, J. E. Structurally similar triphenylphosphine-stabilized undecagolds, Au11 (PPh3) 7Cl3 and [Au11 (PPh3) 8Cl2] Cl, exhibit distinct ligand exchange pathways with glutathione. *J. Am. Chem. Soc.* **2014**, *136*, 13426−13435.

(5) Chen, S.; Fang, W. H.; Zhang, L.; Zhang, J. Atomically Precise Multimetallic Semiconductive Nanoclusters with Optical Limiting Effects. *Angew. Chem., Int. Ed.* **2018**, *57*, 11252−11256.

(6) Guan, Z. J.; Zeng, J. L.; Yuan, S. F.; Hu, F.; Lin, Y. M.; Wang, Q. M. Au57Ag53 (C≡ CPh) 40Br12: a large nanocluster with C1 symmetry. *Angew. Chem., Int. Ed.* **2018**, *57*, 5703−5707.

(7) Weßing, J.; Ganesamoorthy, C.; Kahlal, S.; Marchal, R.; Gemel, C.; Cador, O.; Da Silva, A. C.; Da Silva, J. L.; Saillard, J. Y.; Fischer, R. A. The Mackay-Type Cluster [Cu43Al12](Cp*) 12: Open-Shell 67-Electron Superatom with Emerging Metal-Like Electronic Structure. *Angew. Chem., Int. Ed.* **2018**, *57*, 14630−14634.

(8) Fu, M. L.; Issac, I.; Fenske, D.; Fuhr, O. Metal-Rich Copper Chalcogenide Clusters at the Border Between Molecule and Bulk Phase: The Structures of [Cu93Se42 (SeC6H4SMe) 9 (PPh3) 18], [Cu96Se45 (SeC6H4SMe) 6 (PPh3) 18], and [Cu136S56 (SCH2C4H3O) 24 (dpppt) 10]. *Angew. Chem., Int. Ed.* **2010**, *49*, 6899−6903.
(9) Häkkinen, H.; Abbet, S.; Sanchez, A.; Heiz, U.; Landman, U. Structural, electronic, and impurity-doping effects in nanoscale chemistry: supported gold nanoclusters. *Angew. Chem., Int. Ed.* **2003**, *42*, 1297−1300.
(10) Anker, J.; Hall, W. P.; Lyandres, O.; Shah, N.; Zhao, J.; Duyne, R. Biosensing with Plasmonic Nanosensors. *Nat. Mater.* **2008**, *7*, 442−453.
(11) Ben-Jaber, S.; Peveler, W. J.; Quesada-Cabrera, R.; Cortés, E.; Sotelo-Vazquez, C.; Abdul-Karim, N.; Maier, S. A.; Parkin, I. P. Photo-induced enhanced Raman spectroscopy for universal ultra-trace detection of explosives, pollutants and biomolecules. *Nat. Commun.* **2016**, *7*, No. 12189.
(12) Gruene, P.; Rayner, D. M.; Redlich, B.; van der Meer, A. F.; Lyon, J. T.; Meijer, G.; Fielicke, A. Structures of neutral Au7, Au19, and Au20 clusters in the gas phase. *Science* **2008**, *321*, 674−676.
(13) Woodham, A. P.; Fielicke, A. Superoxide formation on isolated cationic gold clusters. *Angew. Chem., Int. Ed.* **2014**, *53*, 6554−6557.
(14) Kwak, K.; Choi, W.; Tang, Q.; Kim, M.; Lee, Y.; Jiang, D.-e.; Lee, D. A molecule-like PtAu 24 (SC 6 H 13) 18 nanocluster as an electrocatalyst for hydrogen production. *Nat. Commun.* **2017**, *8*, No. 14723.
(15) Bakr, O. M.; Amendola, V.; Aikens, C. M.; Wenseleers, W.; Li, R.; Dal Negro, L.; Schatz, G. C.; Stellacci, F. Silver nanoparticles with broad multiband linear optical absorption. *Angew. Chem., Int. Ed.* **2009**, *48*, 5921−5926.
(16) Makarem, A.; Berg, R.; Rominger, F.; Straub, B. F. A fluxional copper acetylide cluster in CuAAC catalysis. *Angew. Chem., Int. Ed.* **2015**, *54*, 7431−7435.
(17) Karelovic, A.; Ruiz, P. The role of copper particle size in low pressure methanol synthesis via CO 2 hydrogenation over Cu/ZnO catalysts. *Catal. Sci. Technol.* **2015**, *5*, 869−881.
(18) Yang, Y.; Evans, J.; Rodriguez, J. A.; White, M. G.; Liu, P. Fundamental studies of methanol synthesis from CO 2 hydrogenation on Cu (111), Cu clusters, and Cu/ZnO (0001 [combining macron]). *Phys. Chem. Chem. Phys.* **2010**, *12*, 9909−9917.
(19) Liu, C.; Yang, B.; Tyo, E.; Seifert, S.; DeBartolo, J.; von Issendorff, B.; Zapol, P.; Vajda, S.; Curtiss, L. A. Carbon dioxide conversion to methanol over size-selected Cu4 clusters at low pressures. *J. Am. Chem. Soc.* **2015**, *137*, 8676−8679.
(20) Prasad, R.; Singh, P. A review on CO oxidation over copper chromite catalyst. *Catal. Rev.* **2012**, *54*, 224−279.
(21) Wang, L. N.; Li, X. N.; Jiang, L. X.; Yang, B.; Liu, Q. Y.; Xu, H. G.; Zheng, W. J.; He, S. G. Catalytic CO Oxidation by O2 Mediated by Noble-Metal-Free Cluster Anions Cu2VO3−5−. *Angew. Chem., Int. Ed.* **2018**, *57*, 3349−3353.
(22) Fielicke, A.; Kirilyuk, A.; Ratsch, C.; Behler, J.; Scheffler, M.; von Helden, G.; Meijer, G. Structure determination of isolated metal clusters via far-infrared spectroscopy. *Phys. Rev. Lett.* **2004**, *93*, No. 023401.
(23) Wagner, J. P.; McDonald, D. C.; Duncan, M. A. An Argon−Oxygen Covalent Bond in the ArOH+ Molecular Ion. *Angew. Chem., Int. Ed.* **2018**, *57*, 5081−5085.
(24) Kiawi, D. M.; Chernyy, V.; Oomens, J.; Buma, W. J.; Jamshidi, Z.; Visscher, L.; Waters, L.; Bakker, J. M. Water dissociation upon adsorption onto free iron clusters is size dependent. *J. Phys. Chem. Lett.* **2016**, *7*, 2381−2387.
(25) Woodham, A. P.; Meijer, G.; Fielicke, A. Charge separation promoted activation of molecular oxygen by neutral gold clusters. *J. Am. Chem. Soc.* **2013**, *135*, 1727−1730.
(26) Woodham, A. P.; Meijer, G.; Fielicke, A. Activation of molecular oxygen by anionic gold clusters. *Angew. Chem., Int. Ed.* **2012**, *51*, 4444−4447.
(27) Hamilton, S. M.; Hopkins, W. S.; Harding, D. J.; Walsh, T. R.; Gruene, P.; Haertelt, M.; Fielicke, A.; Meijer, G.; Mackenzie, S. R. Infrared induced reactivity on the surface of isolated size-selected clusters: dissociation of N2O on rhodium clusters. *J. Am. Chem. Soc.* **2010**, *132*, 1448−1449.
(28) Parry, I. S.; Kartouzian, A.; Hamilton, S. M.; Balaj, O. P.; Beyer, M. K.; Mackenzie, S. R. Chemical Reactivity on Gas-Phase Metal Clusters Driven by Blackbody Infrared Radiation. *Angew. Chem., Int. Ed.* **2015**, *54*, 1357−1360.
(29) Lushchikova, O. V.; Huitema, D. M.; López-Tarifa, P.; Visscher, L.; Jamshidi, Z.; Bakker, J. M. Structures of Cu n+(n= 3−10) Clusters Obtained by Infrared Action Spectroscopy. *J. Phys. Chem. Lett.* **2019**, *10*, 2151−2155.
(30) Pan, S.; Jana, G.; Merino, G.; Chattaraj, P. K. Noble-noble strong union: Gold at its best to make a bond with a noble gas atom. *ChemistryOpen* **2019**, *8*, 173−187.
(31) Torigoe, H.; Mori, T.; Fujie, K.; Ohkubo, T.; Itadani, A.; Gotoh, K.; Ishida, H.; Yamashita, H.; Yumura, T.; Kobayashi, H.; Kuroda, Y. Direct information on structure and energetic features of Cu+− Xe species formed in MFI-type zeolite at room temperature. *J. Phys. Chem. Lett.* **2010**, *1*, 2642−2650.
(32) Pyykkoe, P. Predicted chemical bonds between rare gases and Au+. *J. Am. Chem. Soc.* **1995**, *117*, 2067−2070.
(33) Michaud, J. M.; Gerry, M. C. XeCu covalent bonding in XeCuF and XeCuCl, characterized by fourier transform microwave spectroscopy supported by quantum chemical calculations. *J. Am. Chem. Soc.* **2006**, *128*, 7613−7621.
(34) Jamshidi, Z.; Eskandari, K.; Azami, S. M. Nature of closed-and open-shell interactions between noble metals and rare gas atoms. *Int. J. Quantum Chem.* **2013**, *113*, 1981−1991.
(35) Jamshidi, Z.; Kaveei, E.; Mohammadpour, M. Investigation of the Electronic Excited States of Small Gold Clusters in Rare Gas Matrices: Spin−Orbit Time-Dependent Density Functional Theory Calculation. *J. Phys. Chem. A* **2015**, *119*, 8579−8587.
(36) Belpassi, L.; Infante, I.; Tarantelli, F.; Visscher, L. The chemical bond between Au (I) and the noble gases. Comparative study of NgAuF and NgAu+ (Ng = Ar, Kr, Xe) by density functional and coupled cluster methods. *J. Am. Chem. Soc.* **2008**, *130*, 1048−1060.
(37) Zeng, T.; Klobukowski, M. Relativistic model core potential study of the Au+ Xe system. *J. Phys. Chem. A* **2008**, *112*, 5236−5242.
(38) Bauschlicher, C. W., Jr.; Partridge, H.; Langhoff, S. R. Comparison of the bonding between ML+ and ML2+ (M= metal, L= noble gas). *Chem. Phys. Lett.* **1990**, *165*, 272−276.
(39) Shayeghi, A.; Johston, R. L.; Rayner, D. M.; Schäfer, R.; Fielicke, A. The nature of bonding between argon and mixed gold−silver trimers. *Angew. Chem., Int. Ed.* **2015**, *54*, 10675−10680.
(40) Jamshidi, Z.; Far, M. F.; Maghari, A. Binding of noble metal clusters with rare gas atoms: Theoretical investigation. *J. Phys. Chem. A* **2012**, *116*, 12510−12517.
(41) Pyykkö, P. Theoretical chemistry of gold. *Angew. Chem., Int. Ed.* **2004**, *43*, 4412−4456.
(42) Read, J.; Buckingham, A. Covalency in ArAu+ and related species? *J. Am. Chem. Soc.* **1997**, *119*, 9010−9013.
(43) Shayeghi, A.; Schäfer, R.; Rayner, D.; Johnston, R.; Fielicke, A. Charge-induced dipole vs. relativistically enhanced covalent interactions in Ar-tagged Au-Ag tetramers and pentamers. *J. Chem. Phys.* **2015**, *143*, No. 024310.
(44) Granatier, J.; Urban, M.; Sadlej, A. J. Van der Waals complexes of Cu, Ag, and Au with hydrogen sulfide. The bonding character. *J. Phys. Chem. A* **2007**, *111*, 13238−13244.
(45) Amsterdam Density Functional Program. http://www.scm.com/.
(46) te Velde, G.; Bickelhaupt, F. M.; Baerends, E. J.; Fonseca Guerra, C.; van Gisbergen, S. J.; Snijders, J. G.; Ziegler, T. Chemistry with ADF. *J. Comput. Chem.* **2001**, *22*, 931−967.
(47) Perdew, J. P.; Burke, K.; Ernzerhof, M. Generalized gradient approximation made simple. *Phys. Rev. Lett.* **1996**, *77*, 3865−3868.
(48) Elmér, R.; Berg, M.; Carlén, L.; Jakobsson, B.; Norén, B.; Oskarsson, A.; Ericsson, G.; Julien, J.; Thorsteinsen, T.-F.;

https://dx.doi.org/10.1021/acs.jpca.0c07771
J. Phys. Chem. A 2020, 124, 9004−9010

Guttormsen, M.; et al. K+ emission in symmetric heavy ion reactions at subthreshold energies. *Phys. Rev. Lett.* **1996**, *77*, 4884−4886.
(49) Grimme, S.; Antony, J.; Ehrlich, S.; Krieg, H. A consistent and accurate ab initio parametrization of density functional dispersion correction (DFT-D) for the 94 elements H-Pu. *J. Chem. Phys.* **2010**, *132*, No. 154104.
(50) Grimme, S.; Ehrlich, S.; Goerigk, L. Effect of the damping function in dispersion corrected density functional theory. *J. Comput. Chem.* **2011**, *32*, 1456−1465.
(51) Becke, A. D.; Johnson, E. R. A density-functional model of the dispersion interaction. *J. Chem. Phys.* **2005**, *123*, No. 154101.
(52) Van Lenthe, E.; Baerends, E. J. Optimized Slater-type basis sets for the elements 1−118. *J. Comput. Chem.* **2003**, *24*, 1142−1156.
(53) Van Lenthe, Ev.; Snijders, J.; Baerends, E. The zero-order regular approximation for relativistic effects: The effect of spin−orbit coupling in closed shell molecules. *J. Chem. Phys.* **1996**, *105*, 6505−6516.
(54) Van Lenthe, E.; Van Leeuwen, R.; Baerends, E.; Snijders, J. Relativistic regular two-component Hamiltonians. *Int J. Quantum. Chem.* **1996**, *57*, 281−293.
(55) Bickelhaupt, F. M.; Baerends, E. J. Kohn-Sham density functional theory: predicting and understanding chemistry. *Rev. Comp. Chem.* **2000**, *15*, 1−86.
(56) Ziegler, T.; Rauk, A. Carbon monoxide, carbon monosulfide, molecular nitrogen, phosphorus trifluoride, and methyl isocyanide as σ donors and π acceptors. A theoretical study by the Hartree-Fock-Slater transition-state method. *Inorg. Chem.* **1979**, *18*, 1755−1759.
(57) Saue, T.; Bast, R.; Gomes, A. S. P.; Jensen, H. J. A.; Visscher, L.; Aucar, I. A.; Di Remigio, R.; Dyall, K. G.; Eliav, E.; Fasshauer, E.; et al. The DIRAC code for relativistic molecular calculations. *J. Chem. Phys.* **2020**, *152*, No. 204104.
(58) Jensen, H. J. Å; Saue, R. B. T.; Visscher, L. et al. A Relativistic ab initio Electronic Structure Program, Release DIRAC18, 2018, http://www.diracprogram.org/.
(59) Sikkema, J.; Visscher, L.; Saue, T.; Iliaš, M. The molecular mean-field approach for correlated relativistic calculations. *J. Chem. Phys.* **2009**, *131*, No. 124116.
(60) Dyall, K. G. Relativistic double-zeta, triple-zeta, and quadruple-zeta basis sets for the 4d elements Y−Cd. *Theor. Chem. Acc.* **2007**, *117*, 483−489.
(61) VandeVondele, J.; Krack, M.; Mohamed, F.; Parrinello, M.; Chassaing, T.; Hutter, J. Quickstep: Fast and accurate density functional calculations using a mixed Gaussian and plane waves approach. *Comput. Phys. Commun.* **2005**, *167*, 103−128.
(62) Goedecker, S.; Teter, M.; Hutter, J. Separable dual-space Gaussian pseudopotentials. *Phys. Rev. B.* **1996**, *54*, 1703−1710.
(63) CP2K Developers Group. http://www.cp2k.org/.
(64) Brehm, M.; Kirchner, B. TRAVIS-a Free Analyzer and Visualizer for Monte Carlo and Molecular Dynamics Trajectories. *J. Chem. Inf. Model.* **2011**, *51*, 2007−2023.
(65) Froudakis, G. E.; Muhlhauser, M.; Farantos, S. C.; Sfounis, A.; Velegrakis, M. Mass spectra and structures of Cu+ Rgn clusters (Rg= Ne, Ar). *Chem. Phys.* **2002**, *280*, 43−51.

https://dx.doi.org/10.1021/acs.jpca.0c07771
J. Phys. Chem. A 2020, 124, 9004−9010